RAPID COMMUNICATIONS

PHYSICAL REVIEW E VOLUME 51, NUMBER 6 JUNE 1995

Halo formation induced by density nonuniformities in intense ion beams

Qian Qian and Ronald C. Davidson
Plasma Physics Laboratory, Princeton University, Princeton, New Jersey 08543

Chiping Chen
Plasma Fusion Center, Massachusetts Institute of Technology, Cambridge, Massachusetts 02139
(Received 21 February 1995)

A test-particle model is used to investigate the charged-particle dynamics in an intense matched ion beam with nonuniform density profile propagating through an alternating-gradient quadrupole magnetic field in the space-charge-dominated regime. It is shown that self-field nonlinearities due to transverse nonuniformities in the beam density not only can result in chaotic ion motion but also can cause halo formation. For heavy-ion fusion applications, these results indicate that accurate density profile control is critical in preventing heavy-ion beams from developing halos.

PACS number(s): 07.77.−n, 29.27.Eg, 41.75.−i, 52.25.Wz

There is a growing interest in the area of advanced high-current ion accelerators for applications such as heavy-ion fusion [1] and nuclear wast treatment [2]. Because the ion beams in these applications are space-charge-dominated, an important aspect in the design of such advanced accelerators and beam transport systems is to find optimal operating regimes in which the emittance growth and beam losses are minimized. For ideal beam focusing systems, a primary source of emittance growth is due to the intrinsic beam space-charge effects. Indeed, Hofmann *et al.* [3] have shown that under certain conditions, the Kapchinskij-Vladimirskij (KV) beam distribution [4,5], the only known collisionless equilibrium for periodically focused intense ion beams, exhibits space-charge-induced instabilities, resulting in emittance growth and possible beam losses.

Recent particle-in-cell (PIC) simulation studies [6] of intense ion beam propagation indicate that mismatched beams develop halos, and that the halo ions can contribute to the emittance growth and are most likely to be lost in the beam transport systems. One of the consequences of halo-induced beam losses is the production of residual radioactivity in the system, so that continuous operation becomes problematic. Several mechanisms for halo development have been proposed [7], including the single-particle–core-interaction model. However, none of these models has been fully validated, both because the presence of numerical noise in the PIC simulations makes a direct verification of halo formation extremely difficult, and also because it is difficult in experiments to single out individual effects that may produce beam halos.

In this paper, use is made of a test-particle model to investigate the dynamics of root-mean-squared (rms) matched, intense ion beams propagating through an alternating-gradient quadrupole magnetic field. The elliptical cross section of the beam is incorporated in the present analysis, assuming that the beam has a parabolic density profile transverse to the propagation direction. A distribution function that is consistent with the assumed density profile is used to specify the initial conditions for the test particles. It is shown that self-field nonlinearities due to the transverse nonuniformity in the beam density profile not only can induce chaotic ion motion [8] but also can lead to halo formation. Because rms beam matching, which does not guarantee necessarily beam matching except for the (ideal) KV beam equilibrium, is widely utilized in the design of accelerator and beam transport systems, the halo formation mechanism reported in this paper is of particular importance.

We consider an rms-matched, continuous, intense ion beam propagating in the z direction through an alternating-gradient quadrupole magnetic field with axial periodicity length S. In the paraxial approximation, the transverse equations of motion for an individual ion can be expressed as [4]

$$\frac{d^2x}{ds^2}+\kappa_q(s)x+\frac{q}{\gamma_b^3\beta_b^2mc^2}\frac{\partial}{\partial x}\phi(x,y,s)=0, \tag{1}$$

and

$$\frac{d^2y}{ds^2}-\kappa_q(s)y+\frac{q}{\gamma_b^3\beta_b^2mc^2}\frac{\partial}{\partial y}\phi(x,y,s)=0, \tag{2}$$

where $s=\beta_b ct$ is the axial coordinate, the periodic function $\kappa_q(s)=\kappa_q(s+S)$ describes the quadrupole focusing field, $\phi(x,y,s)$ and $\beta_b\phi(x,y,s)\vec{e}_z$ are the scalar and vector potentials associated with the space charge and current of the intense ion beam, q and m are the ion charge and rest mass, respectively, c is the speed of light *in vacuo*, $\beta_b c$ is the average axial beam velocity, and $\gamma_b=(1-\beta_b^2)^{-1/2}$ is the relativistic mass factor.

To employ the test-particle model, we determine an analytical expression for the scalar potential, assuming that the beam density profile has the parabolic form

$$n_b(x,y,s)=\begin{cases}\hat{n}_b+\delta\hat{n}_b-2\,\delta\hat{n}_b(x^2/a^2+y^2/b^2) & \text{for } x^2/a^2+y^2/b^2\leq 1,\\ 0 & \text{otherwise.}\end{cases} \tag{3}$$

In Eq. (3), $N=\pi ab\hat{n}_b=\int n_b dxdy=\text{const}$ is the number of ions per unit axial length. The parameter $\delta\hat{n}_b$ is a measure of the nonuniformity of the beam density, and is allowed to be in the range $0\leq\delta\hat{n}_b\leq\hat{n}_b$. The periodic outermost beam envelope functions, $a(s)=a(s+S)$ and $b(s)=b(s+S)$, are to be determined from Eqs. (6) and (7). From the equilibrium Poisson equation, the scalar potential is given by [9]

$$\phi(x,y,s)=-\pi qab\left[\int_0^{\xi}\frac{\hat{n}_b dt}{[(a^2+t)(b^2+t)]^{1/2}}+\int_{\xi}^{\infty}\frac{dt}{[(a^2+t)(b^2+t)]^{1/2}}\int_0^T n_b(T')dT'\right], \tag{4}$$

where $n_b(T)=\hat{n}_b+\delta\hat{n}_b-2\delta\hat{n}_b T$ for $0\leq T\leq 1$, and $n_b(T)=0$ otherwise, and the variable T is defined by

$$T(x,y,t)=\frac{x^2}{a^2+t}+\frac{y^2}{b^2+t}. \tag{5}$$

Here, the function $\xi=\xi(x,y)$ is defined by $T(x,y,\xi)=1$ for any point outside the beam, and by $\xi=0$ for any point inside the beam. After a straightforward but lengthy calculation, a closed analytical expression for $\phi(x,y,s)$ can be obtained for the assumed parabolic-density profile [9].

Making use of the rms beam envelope equations obtained by Sacherer [10] it can be shown that the periodic envelope functions for the rms-matched beam, $a(s)=a(s+S)$ and $b(s)=b(s+S)$, solve the coupled differential equations,

$$\frac{d^2a}{ds^2}+\kappa_q(s)a-\frac{2gK}{a+b}-\frac{g^2\varepsilon_x^2}{a^3}=0, \tag{6}$$

$$\frac{d^2b}{ds^2}-\kappa_q(s)b-\frac{2gK}{a+b}-\frac{g^2\varepsilon_y^2}{b^3}=0, \tag{7}$$

where $K=2q^2N/\gamma_b^3\beta_b^2mc^2$ is the normalized beam perveance, $g=(1-\delta\hat{n}_b/3\hat{n}_b)^{-1}$ is the density shape factor, and ε_x and ε_y are the unnormalized rms emittances in the x and y directions, respectively. Both ε_x and ε_y are taken to be constant because the present test-particle model is aimed at the *onset* of halo formation, where the rms properties of the beam are not expected to vary appreciably.

For a quadrupole focusing channel with the step-function lattice illustrated in Fig. 1(a), the periodic envelope functions $a(s)$ and $b(s)$ are obtained numerically from Eqs. (6) and (7) and are plotted in terms of the rescaled quantities $a(s)/\sqrt{g\varepsilon_x S}$ and $b(s)/\sqrt{g\varepsilon_y S}$ in Fig. 1(b). The choice of system parameters in Fig. 1(b) corresponds to $\eta=0.5$, $\sigma_0=80°$, $\delta\hat{n}_b/\hat{n}_b=0.1$ ($g\cong 1.03$), $SK/\varepsilon_x=10.0$, and $\varepsilon_x=\varepsilon_y$. Here, the parameter η is the filling factor for the step-function lattice [11]; and $\sigma_0^2=S\int_0^S ds[\int_{s_0}^s ds'\kappa_q(s')]^2$ is a measure of the average focusing field strength squared, and is approximately equal to the vacuum phase advance squared [11]. For the case shown in Fig. 1(b), the space-charge-depressed phase advances, as defined by $\sigma_x=g\varepsilon_x\int_0^S ds/a^2(s)$ and $\sigma_y=g\varepsilon_y\int_0^S ds/b^2(s)$, are calculated to be $\sigma_x=12.89°$ and $\sigma_y=12.89°$.

It is important to specify initial conditions for the test-particle motion that are consistent with the density profile assumed in Eq. (3). This is accomplished by the particular choice of initial distribution function at $s=s_0$,

$$f(x,y,x',y',s_0)=\frac{N-\delta N}{\pi^2g^2\varepsilon_x\varepsilon_y}\delta(W-1)+\frac{2\delta N}{\pi^2g^2\varepsilon_x\varepsilon_y}H(W). \tag{8}$$

In Eq. (8), $\delta N\equiv\pi ab\delta\hat{n}_b$, the prime denotes the derivative with respect to s, $\delta(x)$ is the Dirac delta function, $H(x)$ is the function defined by $H(x)=+1$ for $0\leq x\leq 1$, and $H(x)=0$, otherwise, and W is the variable defined by

$$W=\frac{x^2}{a^2}+\frac{1}{g^2\varepsilon_x^2}(ax'-xa')^2+\frac{y^2}{b^2}+\frac{1}{g^2\varepsilon_y^2}(by'-yb')^2. \tag{9}$$

Here, a,a',b,b' denote the "initial" values at $s=s_0$. It is readily verified that $n_b(x,y,s_0)=\int f dx'dy'$ indeed yields the parabolic-density profile in Eq. (3), and that $\pi g\varepsilon_x$ and $\pi g\varepsilon_y$ are the maximum initial areas occupied by the beam particles in the phase planes (x,x') and (y,y'), respectively.

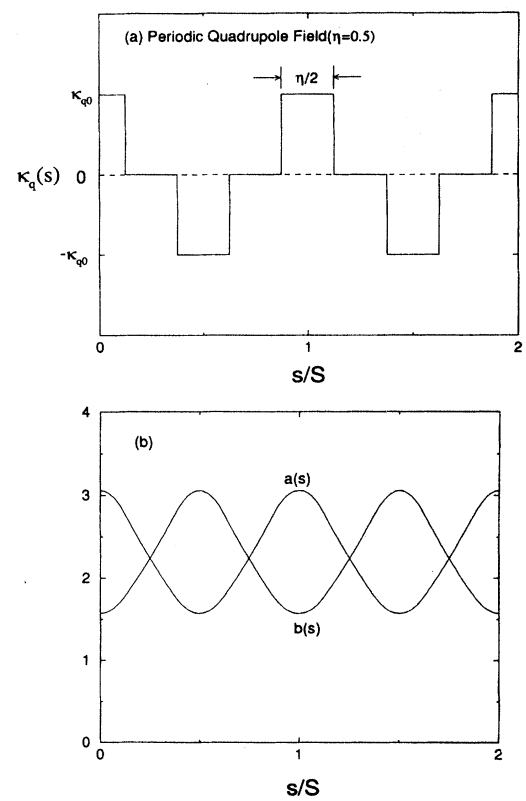

FIG. 1. (a) Lattice function $\kappa_q(s)$ for an alternating-gradient quadrupole magnetic field with periodic step-function profile and filling factor η; and (b) nonlinear periodic envelope functions $a(s)$ and $b(s)$ obtained numerically from Eqs. (6) and (7) for $\eta=0.5$, $\sigma_0=80°$, $\delta\hat{n}_b/\hat{n}_b=0.1$ ($g\cong 1.03$), $SK/\varepsilon_x=10.0$, and $\varepsilon_x=\varepsilon_y$. Here, $a(s)$ and $b(s)$ are plotted in terms of rescaled quantities $a(s)/\sqrt{g\varepsilon_x S}$ and $b(s)/\sqrt{g\varepsilon_y S}$.

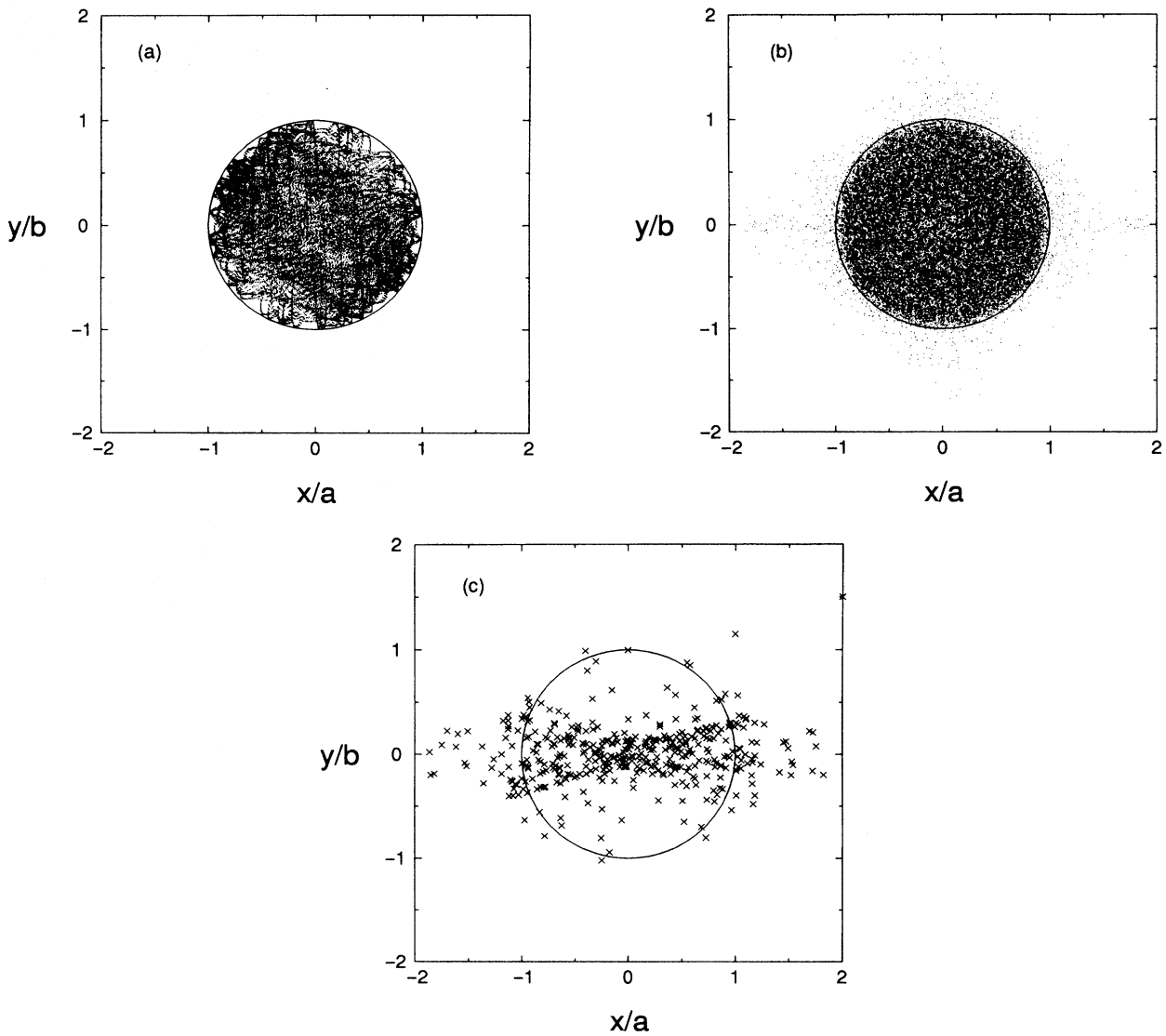

FIG. 2. Poincaré surface-of-section plots for the trajectories of 100 test ions obtained numerically from Eqs. (1) and (2) for propagation over 400 lattice periods. The test ions are loaded initially at $s=s_0$ according to the distribution function in Eq. (8). The two cases correspond to (a) a uniform-density (KV) beam with $\delta\hat{n}_b=0$ ($g=1$), and (b) a parabolic-density beam with $\delta\hat{n}_b/\hat{n}_b=0.1$ ($g\cong1.03$). The system parameters are otherwise the same in both (a) and (b), and are given by $\eta=0.5$, $\sigma_0=80°$, $SK/\varepsilon_x=10.0$, and $\varepsilon_x=\varepsilon_y$. Shown in (c) is the Poincaré surface-of-section plot for the trajectory of a single halo test particle for the case presented in (b).

The dynamical equations (1) and (2) together with Eqs. (3)–(9) completely describe the model and are used subsequently to show halo formation in nonuniform density beams. For $\delta\hat{n}_b=0$ (i.e., for $g=1$), the beam density is uniform and the self-fields have a linear dependence on x and y within the ellipse defined by $(x/a)^2+(y/b)^2=1$, corresponding to the KV beam equilibrium. In this case, Eqs. (1) and (2) reduce to coupled (linear) Hill's equations, and the ion orbits are confined within the beam envelope, provided the latter is stable.

For a *nonuniform* beam with $\delta\hat{n}_b>0$ (i.e., with $g>1$), however, Eqs. (1) and (2) are *nonlinear* due to the nonlinearities in the self-field forces. The ion orbits are nonintegrable and can become chaotic, as shown previously in the constant-radius-envelope approximation [8]. This is also true for periodically varying envelope functions. Because Eqs. (1) and (2) are nonintegrable, numerical analyses prove to be more effective than analytical approaches. In the present analysis, the Adams predictor-corrector scheme [12] is used to integrate numerically Eqs. (1) and (2), where the periodic functions $a(s)$ and $b(s)$ are obtained numerically from the envelope equations (6) and (7). Using the analytical expression for the scalar potential ϕ [9], various benchmark studies have been carried out to assure that the computer roundoff errors are negligibly small and do not affect the results presented below.

Figure 2 shows the Poincaré map of the trajectories of 100 test ions for the phase plane (x,y) as the test ions pass each lattice period, i.e., at $s=0,S,2S,\ldots,400S$. The ions are initially loaded at $s=s_0=0$ according to the distribution func-

tion in Eq. (8) for the choice of system parameters corresponding to $\eta=0.5$, $\sigma_0=80°$, $SK/\varepsilon_x=10.0$, and $\varepsilon_x=\varepsilon_y$. Case (a) corresponds to a uniform-density (KV) beam with $\delta\hat{n}_b/\hat{n}_b=0$ $(g=1)$, while case (b) corresponds to a nonuniform-density beam with $\delta\hat{n}_b/\hat{n}_b=0.1$ $(g\cong 1.03)$. In Fig. 2(a), all of the ion orbits are enclosed within the elliptical beam boundary, i.e., within the solid circle defined by $(x/a)^2+(y/b)^2=1$, as expected for a KV beam. In contrast, Fig. 2(b) shows a tenuous halo of ions surrounding a dense core for the case of a nonuniform-density beam. The dense core is indicated by the solid circle $(x/a)^2+(y/b)^2=1$. It is found that the halo particles can escape from the beam core on a time scale as short as a few lattice periods. Figure 2(c) shows the Poincaré surface-of-section in the phase plane (x,y) for a single halo particle for the case shown in Fig. 2(b). The maximum radial excursion of halo particles in Fig. 2 is about two times the maximum envelope radius for the particular set of parameters chosen in the figure. The nonuniformity threshold condition, $(\delta\hat{n}_b/\hat{n}_b)_c$, for the expulsion of halo particles from the beam core defined by the boundary $x^2/a^2+y^2/b^2=1$ can be smaller than 10% in the parameter region $(\sigma_0,KS/\varepsilon_x)$ of practical interest. More detailed results and analysis, including the phase space structure inside and outside the beam, will be reported in a future article [9].

To summarize, we have shown using a test-particle model that nonlinearities in the self-fields not only can result in chaotic ion motion but also can cause a halo to develop for an intense ion beam propagating through an alternating-gradient quadrupole magnetic field. This is found to be true even when the beam is *matched* in the rms sense in the space-charge-dominated regime which is of considerable practical importance in the design of advanced accelerators. The importance of this mechanism for halo formation, which has long been overlooked, is further elucidated by the fact that the chaotic particle trajectories and the escape of the halo particles from inside the beam are due totally to the nonuniformity in the beam density profile in the present model. For heavy-ion fusion applications, these results indicate that accurate density profile control is critical in preventing heavy-ion beams from developing halos.

The authors express their special thanks to Dr. Robert D. Ryne, who provided valuable assistance in the numerical computations. This work was supported in part by U.S. Department of Energy Contract No. DE-AC02-76-CHO-3073 and in part by the U.S. Office of Naval Research. The research by Chiping Chen was also supported by the U.S. Air Force Office of Scientific Research.

[1] E. P. Lee and J. Hovingh, Fusion Technol. **15**, 369 (1989).
[2] R. A. Jameson, in *Advanced Accelerator Concepts*, edited by J. S. Wurtele, AIP Conf. Proc. No. 279 (AIP, New York, 1993), p. 969.
[3] I. Hofmann, L. Laslett, L. Smith, and I. Haber, Part. Accel. **13**, 145 (1983).
[4] R. C. Davidson, *Physics of Nonneutral Plasmas* (Addison-Wesley, Reading, MA, 1990), Chap. 10, and references therein.
[5] I. Kapchinskij and V. Vladimirskij, in *Proceedings of the International Conference on High Energy Accelerators and Instrumentation* (CERN Scientific Information Service, Geneva, 1959), p. 274.
[6] A. Cucchetti, M. Reiser, and T. P. Wangler, in *IEEE Proceedings of the 1991 Particle Accelerator Conference* (IEEE, New York, NY, 1991), Vol. 1, p. 251.
[7] R. L. Gluckstern, Phys. Rev. Lett. **73**, 1247 (1994).
[8] Q. Qian, R. C. Davidson, and C. Chen, Phys. Plasmas **1**, 1328 (1994).
[9] Q. Qian, R. C. Davidson, and C. Chen, Phys. Plasmas (to be published).
[10] F. J. Sacherer, IEEE Trans. Nucl. Sci. **NS-18**, 1105 (1971).
[11] R. C. Davidson and Q. Qian, Phys. Plasmas **1**, 3104 (1994).
[12] E. Isaacson and H. B. Keller, *Analysis of Numerical Methods* (Wiley, New York, 1966).